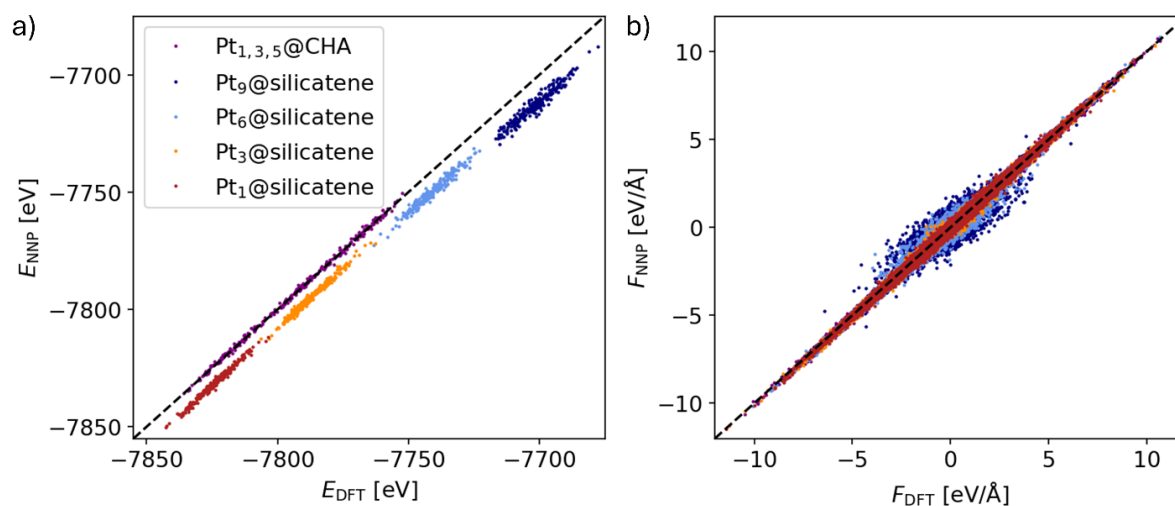


## Supporting Information for: Migration of Zeolite-Encapsulated Subnanometre Platinum Clusters via Reactive Neural Network Potentials

Christopher J. Heard,\* Lukas Grajciar and Andreas Erlebach

### Comparison of DFT and NNP for static calculations



**Figure S1.** Correlation of DFT and NNP calculated energies (a) and forces (b) for all test cases shown in Figure 2.

Previous DFT calculations revealed that the Pt atom preferentially occupies the plane of the six-ring in siliceous LTA framework, and that a similar configuration is stable for other frameworks, including CHA, SOD and RHO (Hou *et al.*, *ACS Catal.*, 10, (2020), p.11057). Hence, the migration dynamics and accessibility of Pt in siliceous six-ring zeolites will be substantially affected by the binding of Pt to the six-ring. We calculated the structure of a 6-ring local minimum for Pt<sub>1</sub>@CHA(six-ring) with both DFT (PBE-D3) and NNP. The NNP is found to reproduce the DFT structure with high fidelity (Figure 1). Table 1 shows the relevant O-Pt and O-Pt-O angles.

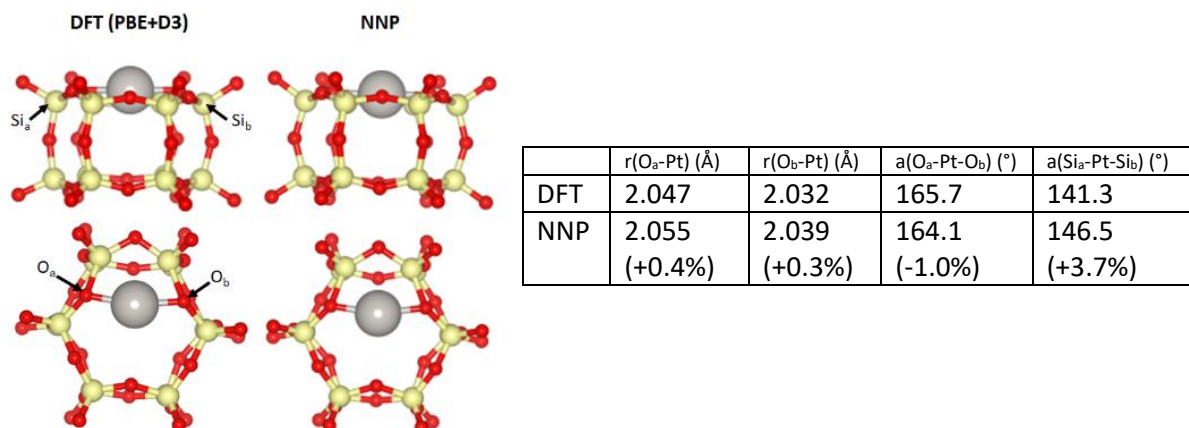


**Figure S2.** Comparison of DFT and NNP predictions for a static Pt<sub>1</sub> local minimum configuration in CHA.

**Table S1.** Mean absolute errors (MAE) of energies and forces for different systems taken from the DFT database and MD production runs.

	RMSE	Energies [meV/atom]	Forces [meV/Å]
Database test set	Silica	2.9	74
	Pt@zeolite	2.2	100
	Pt (gas+bulk)	11.6	79
MD test sets	Pt <sub>1,3,5</sub> @CHA	0.7	76
	Pt <sub>1</sub> @silicatene	7.3	77
	Pt <sub>3</sub> @silicatene	7.4	76
	Pt <sub>6</sub> @silicatene	8.6	82
	Pt <sub>9</sub> @silicatene	11.1	91

### Cell parameters

CHA: 288 atom supercell. a=18.66710 b=18.66710 c=18.66710  $\alpha=94.2604$   $\beta=94.2604$   $\gamma=94.2603$ , volume: 6447.987660 Å<sup>3</sup>

For umbrella sampling a smaller 108 atom supercell was employed, with cell parameters:  
a=14.76700 b=13.67500 c=13.67500  $\alpha=120.0000$   $\beta=90.0000$   $\gamma=90.0000$ , volume: 2391.539699 Å<sup>3</sup>

LTA: 72 atom supercell. a=11.91900 b=11.91900 c=11.91900  $\alpha=90.0000$   $\beta=90.0000$   $\gamma=90.0000$ , volume: 1693.243525 Å<sup>3</sup>

MFI: 288 atom supercell. a=20.00930 b=19.94460 c=13.32000  $\alpha=90.0000$   $\beta=90.0000$   $\gamma=90.0000$ , volume: 5315.711811 Å<sup>3</sup>

TON: 288 atom supercell. a=14.11540 b=17.89950 c=21.02580  $\alpha=90.0000$   $\beta=90.0000$   $\gamma=90.0000$ , volume: 5312.349505 Å<sup>3</sup>

MWW: 432 atom supercell. a=25.00870 b=14.43880 c=25.13420  $\alpha=90.0000$   $\beta=90.0000$   $\gamma=90.0000$ , volume: 9075.848860

### Pt<sub>1</sub> NEB pathway in CHA

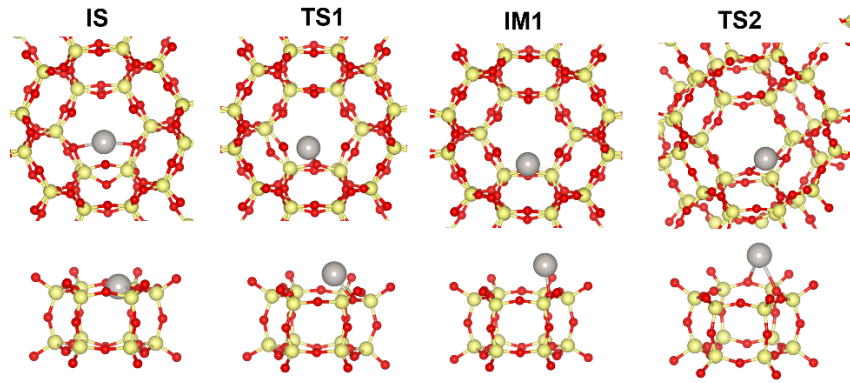
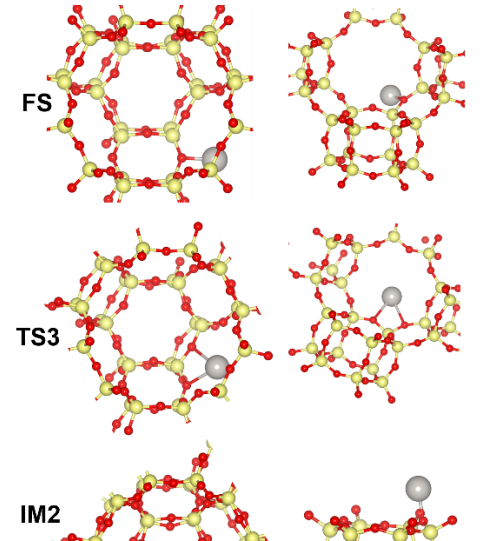
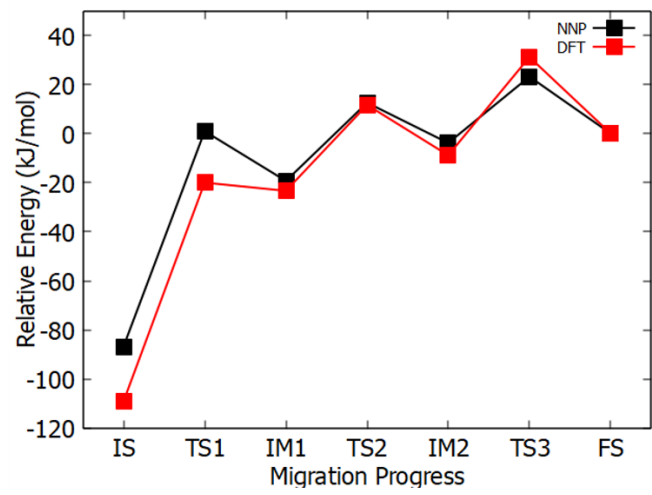
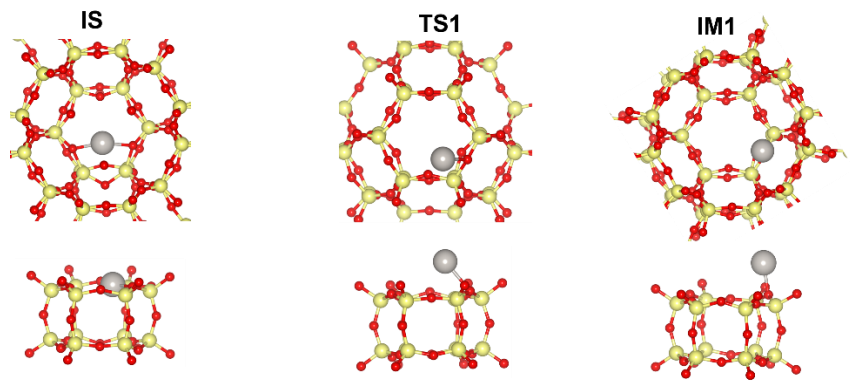
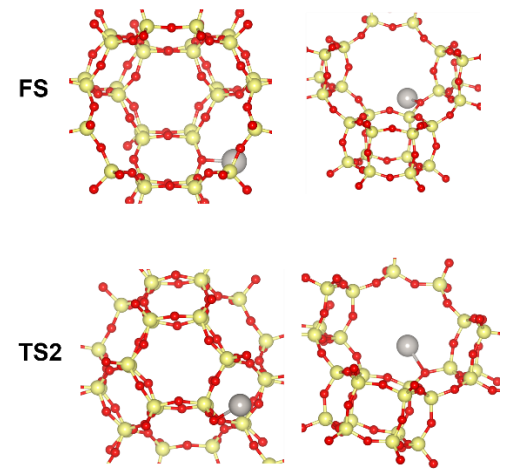
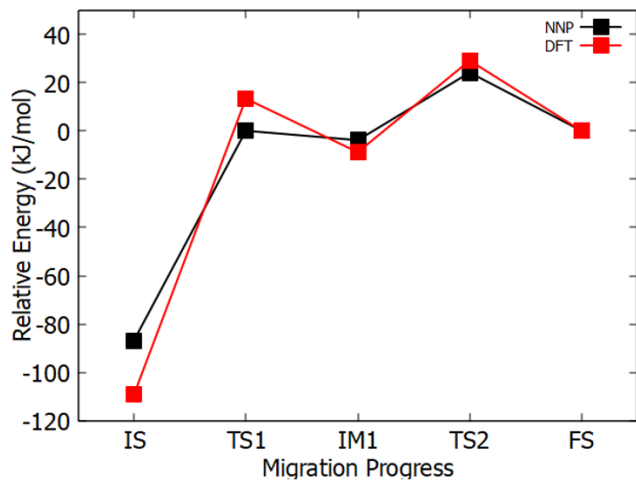


**Figure S3.** Nudged elastic band pathways for Pt<sub>1</sub> diffusion through the 8-ring in CHA. The Pt atom progresses from the plane of the 6-ring, to the 8-ring, then through the 8-ring to the final state via either a two-step pathway (above), or a three step pathway (below), with similar effective barriers. *Above:* The first step involves Pt migration out of the plane of the 6-ring to form a single Pt-O bond ( $r_{\text{Pt-O}} = 2.038 \text{ \AA}$ ) with a framework oxygen atom which bridges a 4-ring, a 6-ring and the 8-ring. The second step is the transfer of Pt through the 8-ring to the nearest oxygen atom in the adjacent cage ( $r_{\text{Pt-O}} = 2.039 \text{ \AA}$ ). *Below:* The first step involves Pt migration out of the plane of the 6-ring to form a single Pt-O bond ( $r_{\text{Pt-O}} = 2.043 \text{ \AA}$ ) with a framework oxygen atom which bridges two 4-rings and the 6-ring. The second step is migration between adjacent framework oxygen atoms, to the site which bridges a 4-ring, the 6-ring and an 8-ring ( $r_{\text{Pt-O}} = 2.038 \text{ \AA}$ ). The final step is the transfer of Pt through the 8-ring to the nearest oxygen atom in the adjacent cage ( $r_{\text{Pt-O}} = 2.039 \text{ \AA}$ ). In both pathways, the rate determining elementary step is the initial transfer of Pt out of the 6-ring. This pathway was not observed to be feasible on the free energy surface. This is likely due to the strong preference for intercage hops through the d6r, and the ease of disruption of the framework by Pt<sub>1</sub>.

### Pt<sub>1</sub> migration through d6r in CHA

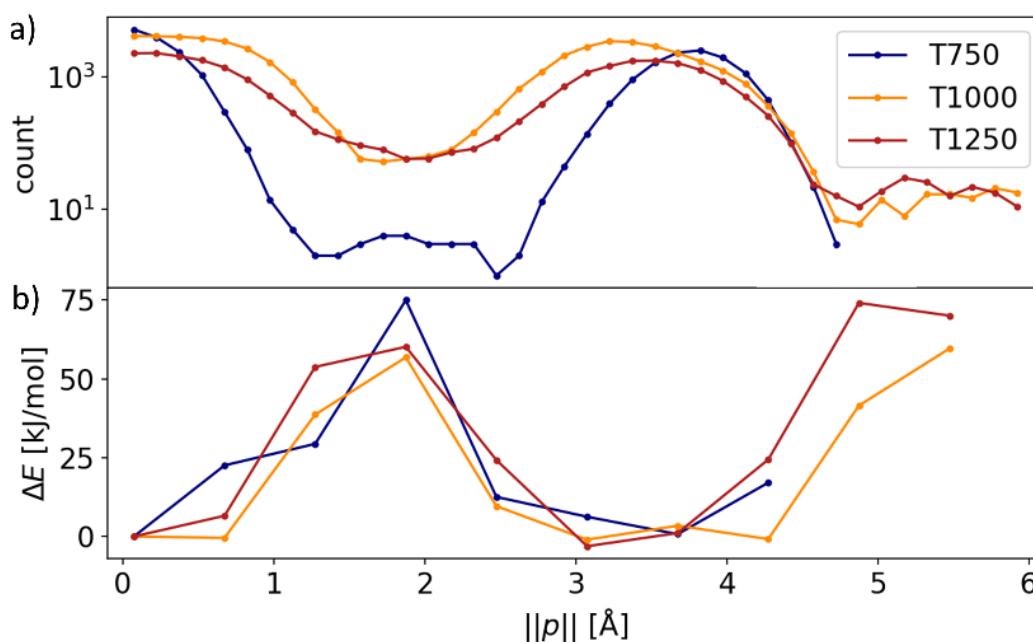


**Figure S4.** Euclidean norm  $||\mathbf{p}||$  of the projected Pt position on the vector connecting the centers of mass of the two single six rings (around 0 and 3 Å on the x-axis) for Pt<sub>1</sub>@CHA: a) histogram of  $||\mathbf{p}||$  for T = 750, 1000, 1250 K and b) energy profile from average energies as a function of  $||\mathbf{p}||$ .

The location and average internal energies were extracted from the NVT MD simulations of Pt<sub>1</sub>@CHA at 750, 1000 and 1250 K, showing that the atom spends a negligible proportion of simulation time in the intermediate space inside the d6r, (between 1-3 Å from the 6R face), but rather occupies the three degenerate states of either 6-ring face. The energies of these intermediate states can be approximately extracted and range from 0.58 to 0.78 eV over the temperature range

considered. These values are in-line with i) the free energy barrier calculated via umbrella sampling at 300 K (0.63 eV), ii) the athermal electronic energy barrier calculated via the nudged elastic band method with the NNP (0.73 eV) and iii) the DFT NEB barrier (0.77 eV).

### Mean Squared Displacement traces for Pt<sub>1</sub>, Pt<sub>3</sub> and Pt<sub>5</sub> in CHA, MFI, TON and MWW

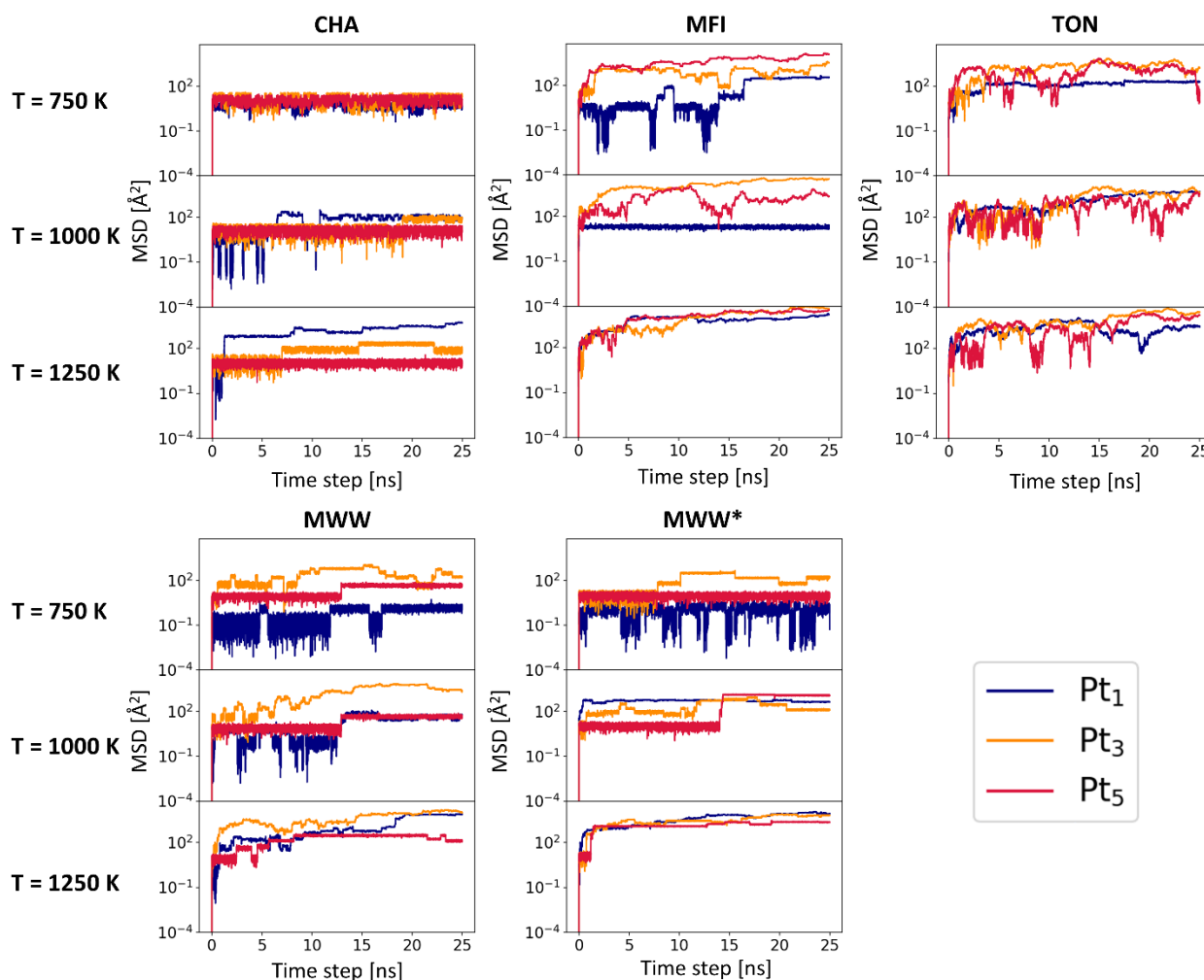


**Figure S5.** Mean squared displacements (MSD) of Pt atoms in CHA, MFI, TON and MWW (with a second initial structure MWW\*) at 750 K, 1000 K and 1250 K. CHA shows a clear hierarchy in migration modes, both across cluster size and temperature. While the largest cluster (Pt<sub>5</sub>) does not leave the cage during the simulation, Pt<sub>3</sub> is able at high temperature to make discrete hops between adjacent cages, with a rate which increases with temperature. Pt<sub>1</sub> is more diffusive than the trimer and pentamer at extreme temperatures, moving between faces of a d6r and occasionally hopping between cages. However, intercage hops are not observed at 750 K or 1000 K for the single atom.

### Umbrella Sampling of Pt<sub>2</sub>, Pt<sub>3</sub> and Pt<sub>4</sub> in LTA

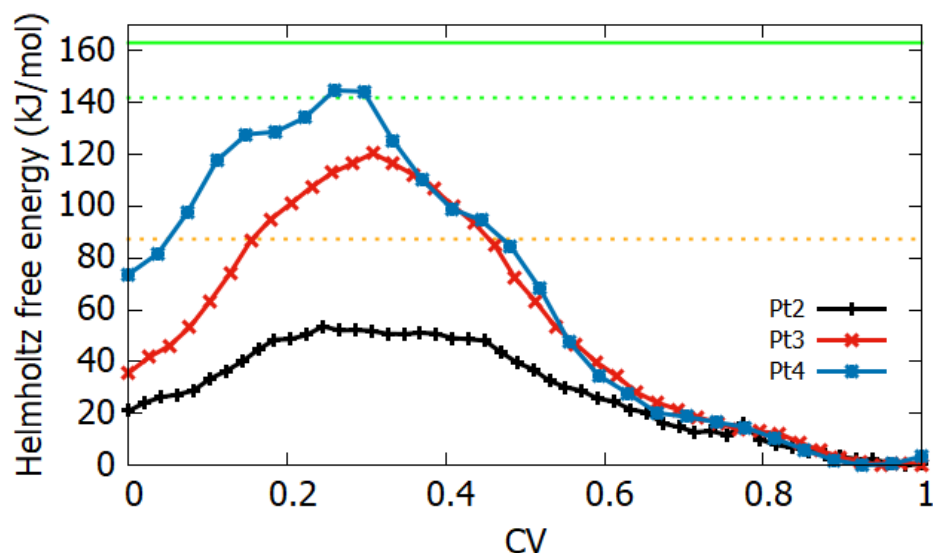


**Figure S6.** Helmholtz free energy profiles for inter-cage cluster migration of Pt<sub>2</sub>, Pt<sub>3</sub> and Pt<sub>4</sub> in LTA from umbrella sampling at 300 K. Energies are given relative to states in the LTA  $\alpha$ -cage at a CV value of 0.6. The x-axis is given in scaled units spanning the range of the chosen CV (Figure S5). We did not find a reasonable free energy pathway for Pt<sub>1</sub> through the 8-ring. The (athermal) NEB barrier for inter-cage migration is included (at NNP level) according to two routes: direct 6-ring to 6-ring transfer via the SOD cage (orange dotted line), and directly through the 8-ring via the pathway from [ACS Catal. 2020, 10, 19, 11057–11068] (green dashed line). The effective DFT barrier from [ACS Catal. 2020, 10, 19, 11057–11068] is shown in solid green. Thus, Pt<sub>1</sub> inter-cage migration is found to preferentially proceed not via the 8-ring but via smaller rings, and is more hindered than dimer migration, in accordance with the findings for CHA.

MD Isosurfaces of Pt<sub>1</sub>, Pt<sub>3</sub> and Pt<sub>5</sub> in CHA, MFI, TON and MWW at 750 K/1000 K

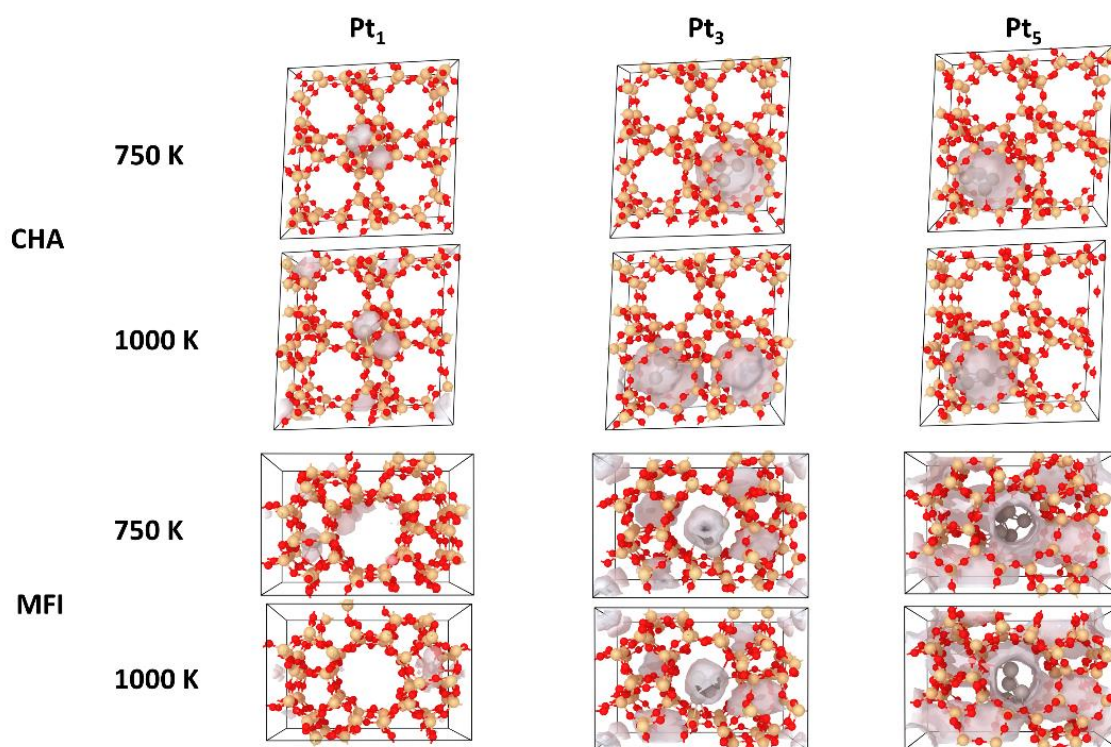
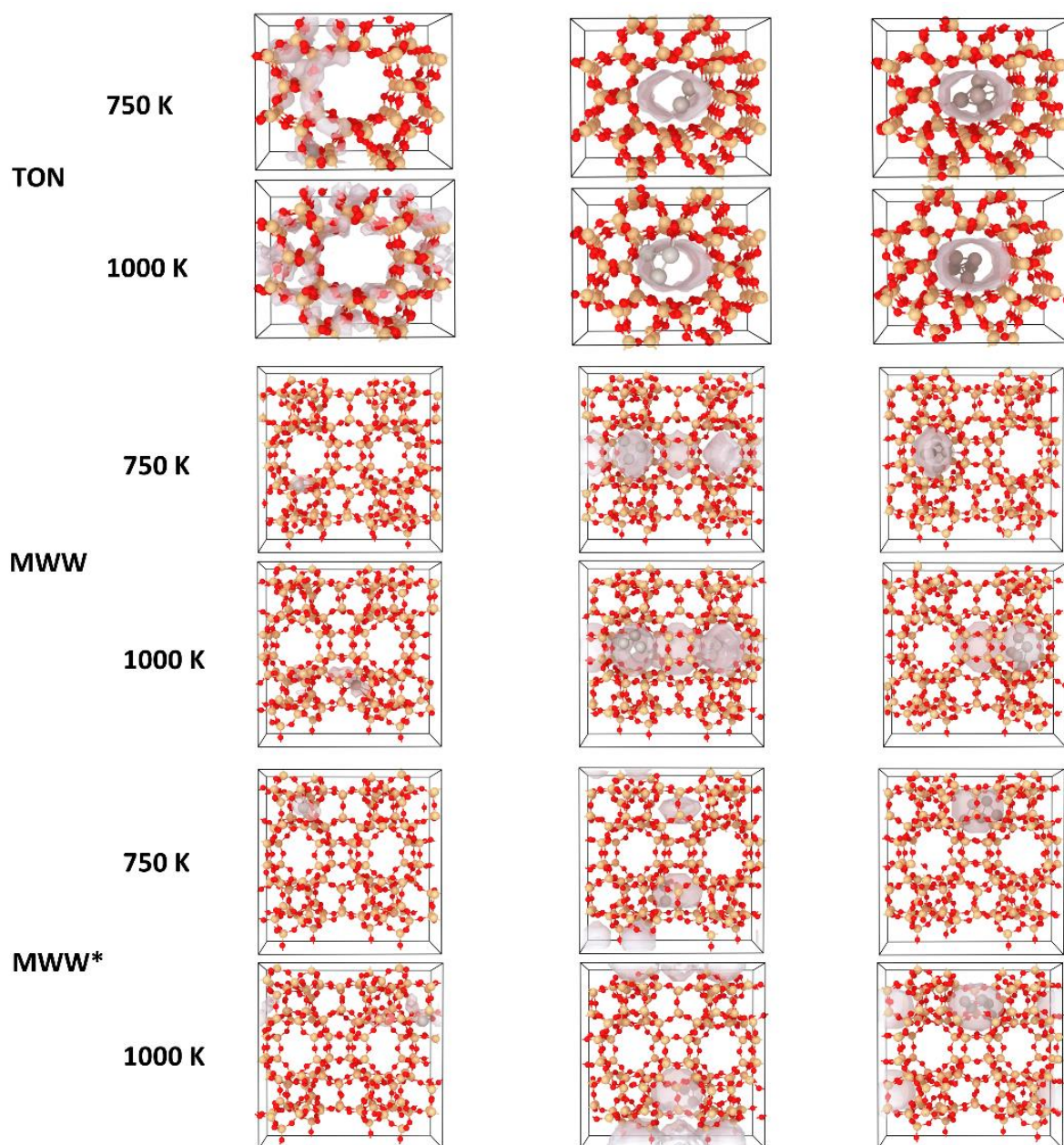
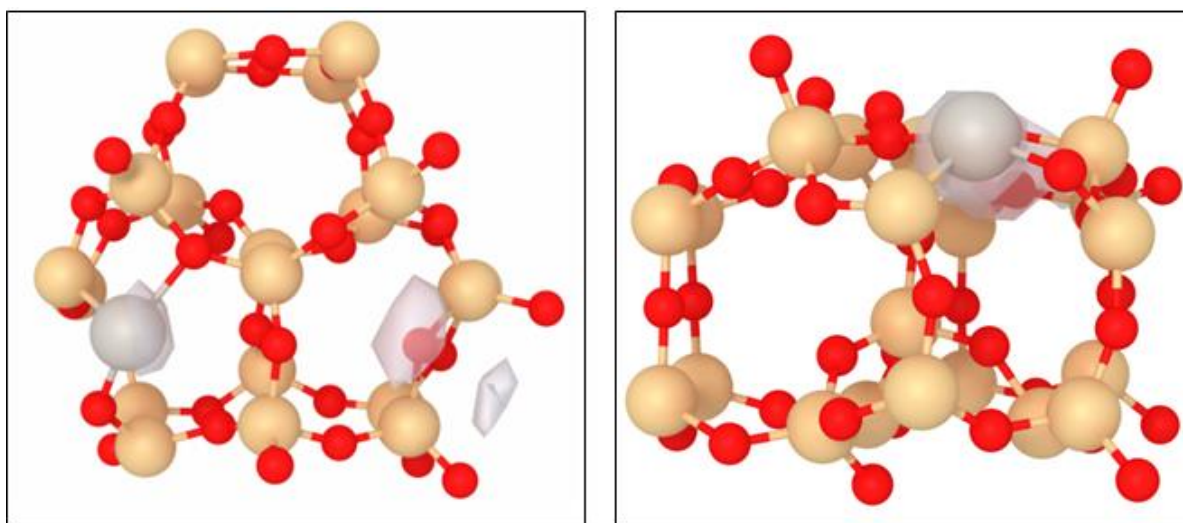


Figure S7. Occupation isosurfaces from MD trajectories of Pt<sub>1</sub>, Pt<sub>3</sub> and Pt<sub>5</sub> in CHA and MFI



**Figure S8.** Occupation isosurfaces from MD trajectories of Pt<sub>1</sub>, Pt<sub>3</sub> and Pt<sub>5</sub> in TON and MWW (with two starting configurations MWW and MWW\*) at 750 K and 1000 K.

### Isosurfaces of Pt<sub>1</sub>@MWW in mel cage



**Figure S9.** Top (left) and side (right) views of the mel cage in Pt<sub>1</sub>@MWW, with isosurfaces from MD at 1250 K. Pt is observed to bind to the 5-ring of the mel cage, breaking an Si-O bond.

### Isosurfaces of Pt<sub>1</sub> and Pt<sub>3</sub> in TON at 1250 K

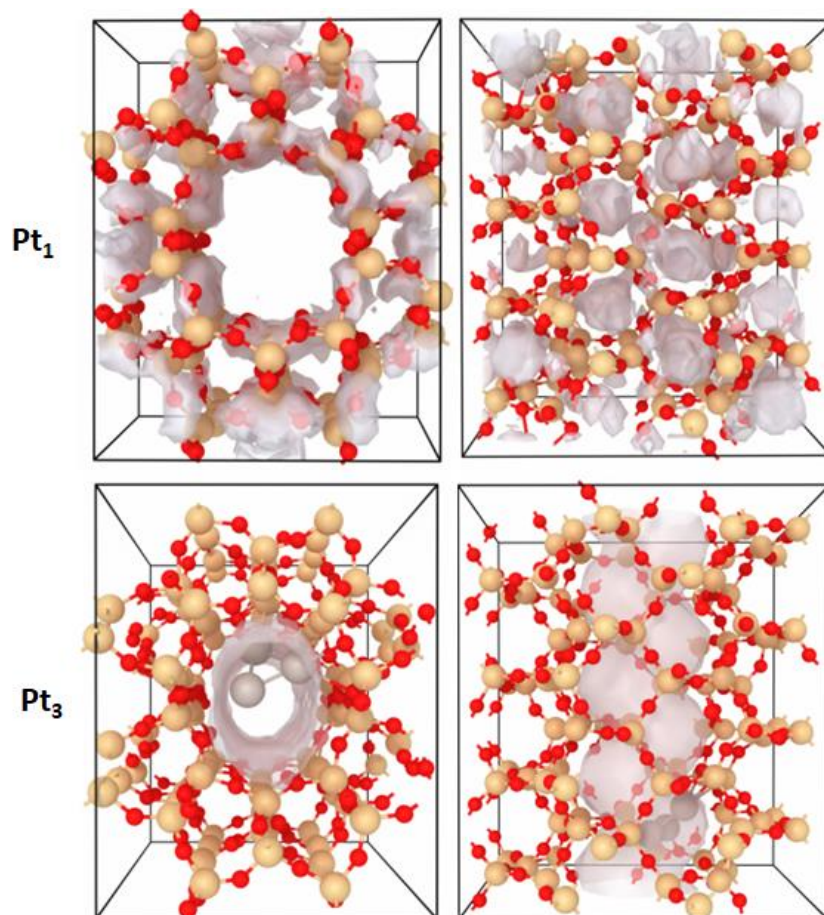


**Figure S10.** Isosurfaces of Pt<sub>1</sub> (top) and Pt<sub>3</sub> (bottom) in TON from a 25 ns simulation MD at 1250 K. Left) view along the 1D channel. Right) View perpendicular to the channel. For Pt<sub>1</sub>, the preferential occupation of the planes of small rings over pore space is clear. For Pt<sub>3</sub>, the cluster describes the shape of the 1D channel, forming a zigzag path along the pore, with no occupation density in the dense region of the framework.

### Collective Variable for Inter-cage cluster migration

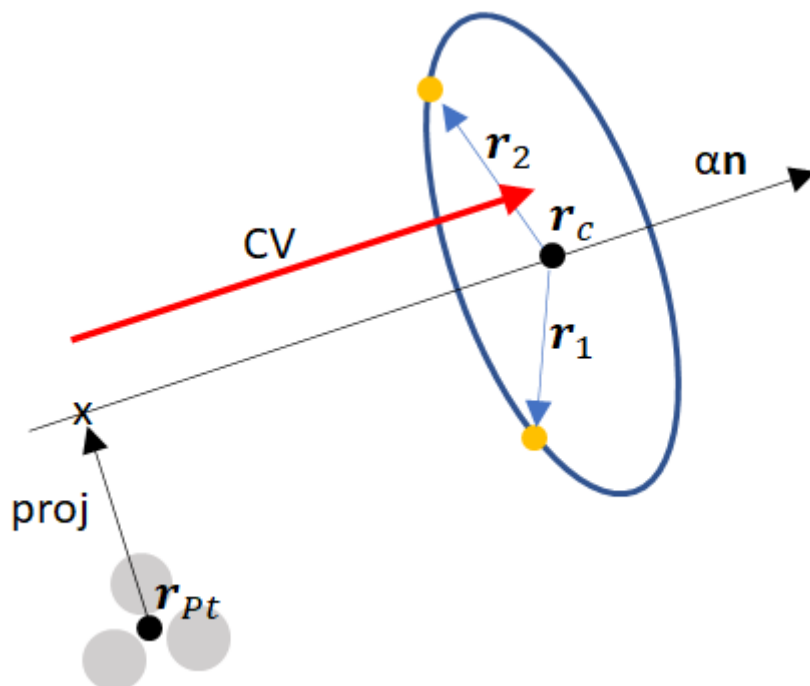


**Figure S11.** Definition of the collective variable (CV) for inter-cage migration via the 8-ring (blue oval). The CV is defined as the distance between the centre of mass of the 8-ring  $r_c$  and the perpendicular projection ( $x$ ) of the centre of mass of the Pt cluster  $r_{Pt}$  onto the vector normal to the 8-ring, passing through  $r_c$ . The normal vector  $n$  is defined as:

$$\mathbf{n} = \frac{1}{\|\mathbf{n}\|} \mathbf{r}_1 \times \mathbf{r}_2$$

where  $\mathbf{r}_j = \mathbf{r}_{Si(j)} - \mathbf{r}_c$

for two selected silicon atoms in the 8-ring. CV ranges presented herein are between -2 and 5 Å.